Universal and nonuniversal aspects of vortex reconnections in superfluids

Alberto Villois and Davide Proment

School of Mathematics, University of East Anglia, Norwich Research Park,
Norwich NR4 7TJ, United Kingdom

Giorgio Krstulovic

Université de la Côte d'Azur, OCA, CNRS, Lagrange, Boîte Postale 4229, 06304 Nice Cedex 4, France

Insight into vortex reconnections in superfluids is presented, making use of analytical results and numerical simulations of the Gross-Pitaevskii model. Universal aspects of the reconnection process are investigated by considering different initial vortex configurations and making use of a recently developed tracking algorithm to reconstruct the vortex filaments. We show that during a reconnection event the vortex lines approach and separate always according to the time scaling $\delta \sim t^{1/2}$ with prefactors that depend on the vortex configuration. We also investigate the behavior of curvature and torsion close to the reconnection point, demonstrating analytically that the curvature can exhibit a self-similar behavior that might be broken by the development of shocklike structures in the torsion.

I. INTRODUCTION

Reconnections in fluids have been a subject of study for a long time in the context of plasma physics [1] and both classical [2] and superfluid dynamics [3]. Depending on the physical system considered, such reconnections are events characterized by a rearrangement in the topology of either a magnetic field (magnetic reconnections) or vorticity field (vortex reconnections). Such topological modifications are believed to play a fundamental role in several physical phenomena such as eruptive solar events [4], energy transfer and fine-scale mixing [5], and turbulent states in superfluids [6]. Despite their physical relevance, reconnections represent also a stand-alone mathematical problem, related, for instance, to the presence of singularities in the Euler equation [2,7,8].

In classical fluids described by the Navier–Stokes-type equations, reconnecting vortex tubes stretch and deform, leading to complicated dynamics and the formation of structures like vortex bridges [5]. In order to understand fundamental aspects of vortex reconnections it is often desirable to work with a vortex configuration where the vorticity is confined along lines of zero core size. Such idealization is called a vortex filament. This limit naturally arises in superfluids such as superfluid liquid helium (He II) and Bose-Einstein condensates (BECs). Superfluids are in fact examples of ideal flows of quantum mechanical nature characterized by the lack of viscous dissipation and by a Dirac δ vorticity distribution supported on the vortex filaments. For such fluids, the velocity circulation is equal to a multiple of the Feynman-Onsager quantum of circulation $\Gamma = h/m$, with h the Planck constant and m the mass of the superfluid's bosonic constituents.

Due to Kelvin's circulation theorem (or Alfvèn's theorem in magnetohydrodynamics), in a barotropic ideal flow reconnections should be forbidden since the circulation of vortex lines transported by the flow is conserved and so their topology is frozen. However, as already suggested by pioneering works of Feynman [9] and Schwarz [10], vortex reconnections in superfluids do exist and play a fundamental role in superfluid turbulence. This was indeed confirmed by Koplik and Levine [3], who performed numerical simulations of reconnecting vortex lines within the Gross-Pitaevskii (GP) model. They showed that Kelvin's circulation theorem does not hold in this context because the superfluid density identically vanishes at the vortex filament. With the progress of experimental techniques in the past decade, reconnecting superfluid vortices have been visualized

in He II [6,11] and in BECs [12,13]. From the theoretical side, many works have been devoted to study the reconnecting vortex filaments in superfluids, by using either the so-called vortex filament (VF) model introduced by Schwarz [10] or the GP model.

The simplest question to ask, although contradictory answers appear in the literature, is related to the rates of approach and separation of two reconnecting vortices. Assuming that a reconnection event is a local process in space and the circulation Γ is the only relevant dimensional quantity involved, by simple dimensional analysis it follows that the distance $\delta(t)$ between two reconnecting filaments should scale as

$$\delta(t) \sim (\Gamma t)^{1/2}, \tag{1}$$

independently if it is measured before or after the reconnection. Such a prediction has been confirmed by numerical simulations of the VF model [14] and in He II experiments [11]. In the framework of the GP model, the same scaling was asymptotically derived in Ref. [15], but a number of numerical studies report disparate scaling exponents that may differ between the before and after reconnection stages [16–18]. Another fundamental question regards the universality of the geometrical shape of the vortex filaments at the reconnection. It is expected that vortices become locally antiparallel during the reconnection process [15]. However, using the VF model, it has been reported that the reconnection angle may follow a broad distribution that depends on the turbulent regime that is considered [14]. It has also been observed that during a reconnection event cusps are generated on the filaments and argument has been given either in favor of those cusps being universal [19] or not [20]. Finally, a great deal of interest has arisen recently in the generation of Kelvin waves (helical waves propagating along vortex filaments) [6,21–23] and the evolution of hydrodynamical helicity [24–28] during reconnection events.

The VF model is based on Biot-Savart equations that describe a regularized Dirac δ vorticity distribution field in the incompressible Euler equation; it provides direct information on the vortex filaments and is widely used to mimic superfluid vortex dynamics and turbulence in He II. However, due to Kelvin's circulation theorem in the Euler equation, reconnections here need to be added by some *ad hoc* cut-and-connect mechanisms. In addition, the VF model introduces a small-scale cutoff to regularize Biot-Savart integral divergence and thus cannot explore the vortex dynamics at the smallest scales where the reconnection events take place. The GP model represents an alternative in the study of vortex dynamics and reconnections, the main advantages being that it naturally contains vortex reconnections in its dynamics and that the entire reconnection process is regular due to the identically zero superfluid density field at the vortex core. Studying such small-scale dynamics is crucial for understanding how energy is transferred through scales and eventually dissipated. Unfortunately, no information can be directly inferred from the GP model on the vortex dynamics because this model described the evolution of an *order parameter* complex field, which contains simultaneously sound excitations and vortex lines in the form of topological defects. We will present here a detailed study of vortex reconnections by exploiting a recently developed tracking algorithm [29] that is able to track vortex filaments in numerical simulations of the GP model with a machine epsilon level of accuracy.

In order to understand what is universal in vortex filament reconnection mechanisms, we study the dynamics of four different initial configurations: (a) perpendicular and (b) almost antiparallel lines, (c) a trefoil knot, and (d) reconnections occurring in a fully turbulent tangle dynamics. We will show that reconnecting vortex lines always obey the dimensional analysis scaling (1) (both before and after reconnection) and they generally separate faster than they approach. In addition, we report that, regardless of the initial configuration, vortices become antiparallel at the reconnection. We also report a self-similar behavior of the curvature close to the reconnection point when torsion does not play an important role and shocklike structures appear in the torsion evolution for some configurations. Those findings are explained by some asymptotic calculations.

II. THE GP MODEL AND RECONNECTION CASE STUDIES

The GP model is a dispersive nonlinear wave equation describing the dynamics of the order parameter ψ of a BEC arising in dilute Bose gases; for the sake of completeness and clarity we introduce it in Appendix A. When ψ is linearized about a constant value $\psi_0 = \sqrt{\rho_0/m}$, the sound velocity results in $c = \sqrt{g\rho_0}/m$ and dispersive effects take place at length scales smaller than the healing length $\xi = \hbar/\sqrt{2\rho_0 g}$. This can be easily understood by rewriting the GP model using those physical parameters

$$i\frac{\partial \psi}{\partial t} = \frac{c}{\sqrt{2}\xi}\left(-\xi^2 \nabla^2 \psi + \frac{m}{\rho_0}|\psi|^2 \psi\right) \tag{2}$$

and comparing the magnitude of the first and second terms on the right-hand side. Note also that by a suitable time and space rescaling, the parameters c and ξ can be reabsorbed; in this work length and time scales are expressed in units of the healing length ξ and its characteristic time $\tau = \xi/c$.

The relationship between the GP equation and a hydrodynamical model is immediately illustrated by introducing the Madelung transformation

$$\psi(\mathbf{x},t) = \sqrt{\frac{\rho(\mathbf{x},t)}{m}}e^{i[\varphi(\mathbf{x},t)/\sqrt{2}c\xi]}, \tag{3}$$

which relates ψ to an inviscid, compressible, irrotational, and barotropic superfluid of density $\rho(\mathbf{x},t)$ and velocity $\mathbf{v} = \nabla\varphi$. In the domain where the Madelung transformation is well defined ($\psi \neq 0$), the velocity field is potential. However, vortices may exist as topological defects of the order parameter. In places where the density vanishes (nodal lines) $\arg\psi$ is not defined. The field ψ still remains a single-value function if the circulation $\oint \mathbf{v} \cdot d\ell$ along a nodal line is a multiple of the quantum of circulation $\Gamma = h/m = 2\sqrt{2}\pi c\xi$. For this reason nodal lines of ψ are called quantum (or quantized) vortices. Their corresponding velocity field $\mathbf{v}$ thus decays as the inverse of the distance to the vortex and their vorticity is therefore a Dirac-supported distribution. Their typical vortex core size is order of ξ.

The GP equation (2) is numerically integrated with a pseudospectral code. The resolution is chosen carefully to sufficiently resolve the vortex core in space and the reconnections in time. We consider four different initial configurations in a cubic box of size L with N collocation points in each dimension.

(a) Perpendicular lines. The order parameter field is characterized by straight vortex filaments perpendicular to each other and having an initial distance of 6ξ. This initial configuration is shown in Fig. 1(a1) for $L/\xi = 128$ and $N = 256$.

(b) Antiparallel lines. Vortex filaments with opposite circulation are set at an average distance of 6ξ. In order to trigger a Crow instability [30], a small perturbation is introduced by adding a Kelvin wave of amplitude ξ and wavelength equal to the system size. The initial configuration is shown in Fig. 1(b1) for $L/\xi = 128$ and $N = 256$.

(c) Trefoil knot. A vortex filament reproducing a torus $\mathcal{T}_{2,3}$ knot (a trefoil) is produced following [31]; the torus on which the knot is built has toroidal and poloidal radii of $R_0 = 16\xi$ and $R_1 = 4\xi$, respectively. The initial configuration is shown in Fig. 1(c1) for $L/\xi = 128$ and $N = 256$.

(d) Turbulent tangle. We prepare an initial condition consisting of several large-scale vortex rings that replicates a Taylor-Green flow as in Ref. [32]. The initial condition then evolves in time: The rings reconnect, breaking the initial symmetry and creating a dense turbulent tangle displayed in Fig. 1(d1) (see [33] for a complete description of the field evolution). We study four successive vortex reconnection events occurring in a small volume [Fig. 1(d2)] at stages when the tangle density is higher for $L/\xi = 256$ and $N = 256$.

The time stepping scheme for cases (a) and (b) is a Strang-splitting method, whereas for cases (c) and (d) it is a second-order Runge-Kutta method. In each case, the time step is chosen to be smaller than the fastest linear time scale of the system. Conservation of the invariants has been carefully checked.

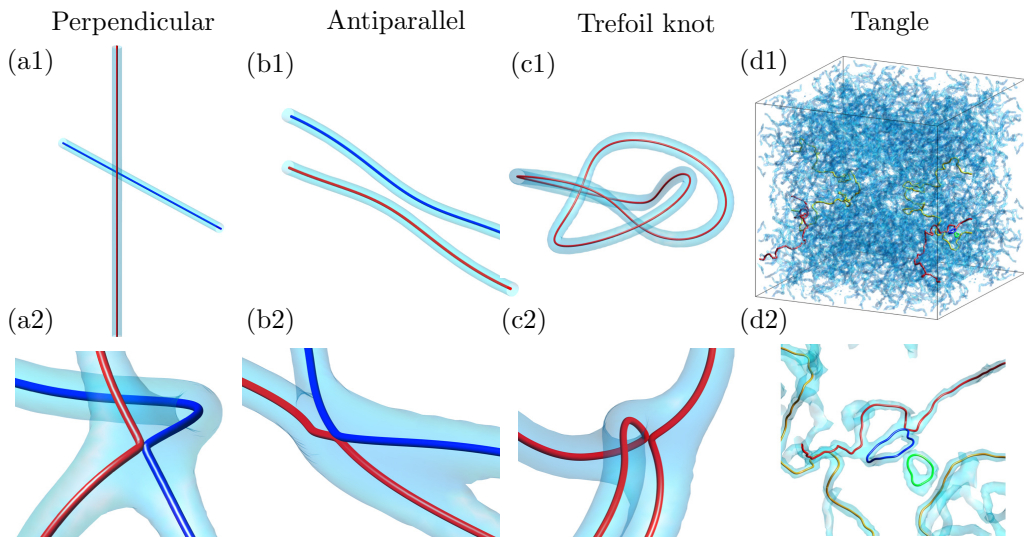Perpendicular   Antiparallel   Trefoil knot   Tangle

FIG. 1. Three-dimensional plot showing the reconnection events explored numerically. The initial configuration is displayed for (a1) the perpendicular vortex lines, (b1) the antiparallel lines, and (c1) the trefoil knot. (a2)–(c2) show a corresponding zoom at the moment of reconnection. Also shown are (d1) the turbulent tangle and (d2) a zoom in of where a reconnection takes place. Red and blue correspond to the reconnecting vortex filaments; the light blue isosurfaces render the density field at low values.

III. APPROACH AND SEPARATION RATES

Apart from the characteristic length scale ξ inherently present in the GP model, when quantized vortices are considered, the quantum of circulation Γ can be used to formulate an extra length scale. Hence, by dimensional analysis, the distance between two reconnecting lines is expected to be

$$\delta^{\pm}(t) = A^{\pm}\xi^{1-2\alpha^{\pm}}|\Gamma(t-t_r)|^{\alpha^{\pm}}, \tag{4}$$

where $\alpha^{\pm}$ and $A^{\pm}$ are dimensionless parameters and the superscript $\pm$ stands for before ($-$) and after ($+$) the reconnection event. The temporal evolution of the minimal distances between reconnecting filaments for the different case studies is displayed in Figs. 2(a)–2(d). An explanatory movie of the knot reconnection is also provided as Supplemental Material [34]. Remarkably, in all cases the approach and separation rates follow the same dimensional $t^{1/2}$ scaling. For each event we estimate the reconnection time t_r by doing a linear fit on $\delta^{\pm}(t)^2$ and compute t_r as the arithmetic mean between $t_r^{\pm}$ that satisfies $\delta^{\pm}(t_r^{\pm})^2 = 0$. The $t^{1/2}$ scaling extends beyond ξ and only slight deviations are observed in some cases. Perhaps this fact could explain the different results for the scaling obtained in Refs. [16–18], where it was concluded that the exponents before and after the reconnection are different. For instance, in Ref. [16] it was found that $\alpha^- \in (0.3, 0.44)$ and $\alpha^+ \in (0.6, 0.73)$ and in Ref. [18] that either $\alpha^{\pm} = 1/2$ or $\alpha^- = 1/3$ and $\alpha^+ = 2/3$, depending on the initial vortex filament configuration. In these works the time asymmetry was interpreted as a manifestation of the irreversible dynamics due to sound emission; we will return to this interesting point in Sec. VI. Let us stress that the tracking algorithm we used is able to measure the intervortex distances even in the presence of sound waves (the Taylor-Green tangle analyzed contains moderate sound at all scales) and no asymmetry concerning the exponent is observed.

Although the measured exponent is always $\alpha^{\pm} = 1/2$, the full dynamics is not symmetrical with respect to the reconnection time as it can be immediately deduced by observing Fig. 2. By estimating the prefactors $A^{\pm}$ with a fit, shown in Fig. 3(a), we conclude that these are always order of the unity but are not universal. Moreover, we observe that the vortex filaments usually separate faster than they approach ($A^- \lesssim A^+$).
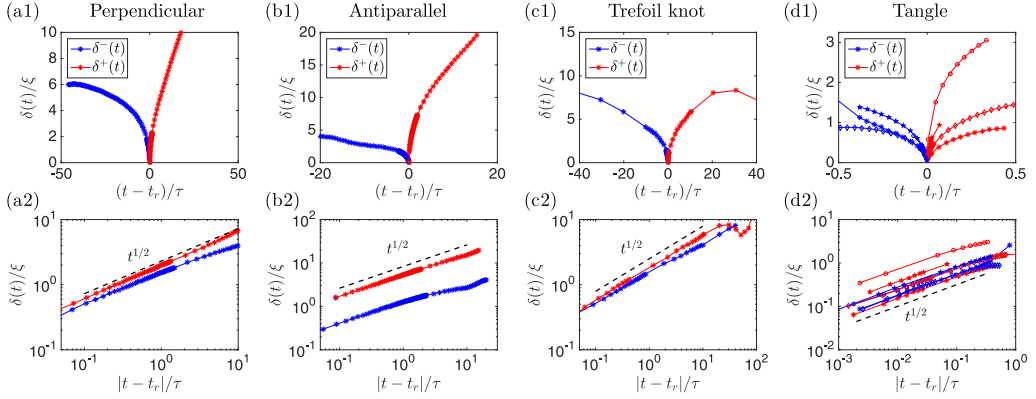
FIG. 2. Temporal evolution of the distance between the reconnecting vortex filaments before (blue) and after (red) the estimated reconnection time t_r for the (a) perpendicular, (b) antiparallel, (c) trefoil knot, and (d) turbulent tangle configurations. For the turbulent tangle four different reconnection events have been tracked. (a2)–(d2) Same plots as in (a1)–(d1) but on a log-log scale.

The tracking algorithm we use follows the pseudovorticity and naturally provides the orientation of the filament with respect to the circulation. It thus allows us to compute the tangent vectors to the lines and infer the orientation of the filaments by evaluating the cosine of the angle θ between the vectors at the two closest points as illustrated in Fig. 3(b) and in Ref. [34]. By approaching
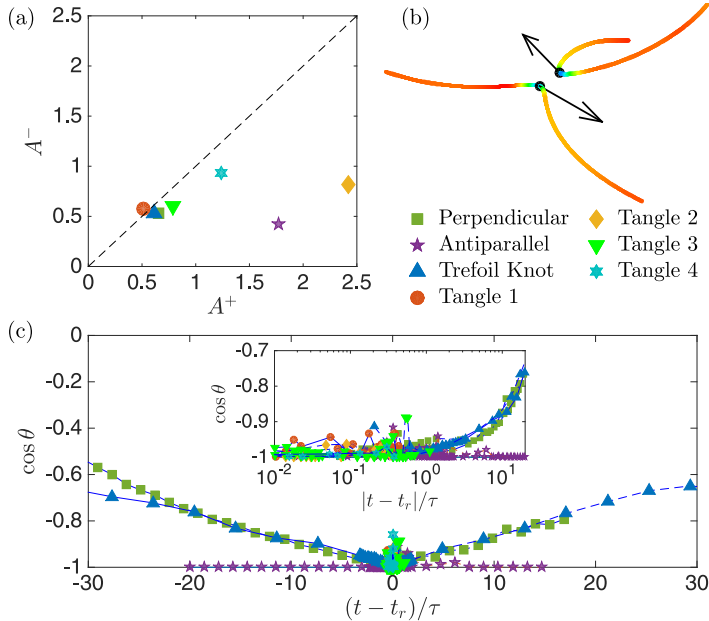

FIG. 3. (a) Fitted values of the prefactors $A^{\pm}$ corresponding to (4). (b) Example of reconnecting filaments (trefoil knot case). The black dots represent the points of minimal distances and are used to compute $\delta(t)$, the arrows are the tangents of the filaments at those points, and the reconnection angle θ is defined by using the scalar product of the tangents. The coloring is proportional to the filament curvature (low in red and high in green and blue). (c) Temporal evolution of the cosine of the reconnecting angle. The inset displays the same plot on a log-log scale.

the reconnection point each vortex filament develops a cusplike structure characterized by high and localized values of the curvature (displayed in green and blue). The temporal evolution of $\cos\theta$ for all the case studies is presented in Fig. 3(c). It is apparent that, independently of the initial configurations, vortices are always antiparallel at the reconnection point. This behavior appears to be time symmetric about the reconnection time and is smooth, as highlighted in the inset of Fig. 3(c), where we show $\cos\theta$ in log-lin coordinates for a better view of the short times before and after reconnection.

IV. ANALYTICAL PREDICTIONS USING A LINEAR APPROXIMATION

The results presented in Figs. 2 and 3 support the analytical predictions obtained by Nazarenko and West in Ref. [15]. Their seminal calculations consider a planar reconnection of two vortex filaments having a hyperbolic configuration at times close to t_r. As we will observe in the following, vortex reconnections do not always fully lie in a plane and the local torsion of the filament can play an important role. We generalize here the calculations performed in Ref. [15], including torsion of the vortex lines to understand its effect during the reconnection. Let us assume that at the reconnection time t_r and close to the reconnection point the order parameter of two reconnecting nonplanar vortex lines is given by

$$\psi_r(x,y,z) = z + \frac{\gamma}{a}(x^2 + y^2) + i(az + \beta x^2 - y^2), \tag{5}$$

with $a \neq 0$ and $\frac{\beta - \gamma}{\gamma + 1} > 0$ (the Nazarenko-West reconnecting vortex profile is recovered by setting $\gamma = 0$). In the vicinity of the vortex filaments, ψ is small and the nonlinear term in Eq. (2) can be neglected. Within this approximation the pre- and postreconnection solution is given by $\psi(x,y,z,t) = e^{[i(t-t_r)\Gamma/4\pi]\nabla^2}\psi_r(x,y,z)$. By solving $\psi(x,y,z,t) = 0$ we can explicitly obtain the temporal evolution of the vortex lines. Equation (4) is obtained with

$$\alpha^+ = \alpha^- = \frac{1}{2}, \quad \frac{A^+}{A^-} = \sqrt{\frac{1 + \gamma}{\beta - \gamma}} \tag{6}$$

for $a > 0$ and $\beta < 1 - 2\gamma/a^2$ (refer to Appendix C for a figure of the vortex profiles, details on the above calculations, and different choices of a and β). Interestingly, the angle between the asymptotes of the hyperbolic vortex configuration close to reconnection is found to be $\phi = 2\tan^{-1}(A^-/A^+)$.

The linear approximation also allows for computing the curvature and torsion of the vortex lines. As pointed out by Schwarz in Ref. [10], the curvature $\kappa^\pm(s,t)$ should present a self-similar behavior close to the reconnection point of the form $\kappa^\pm(s,t) = \kappa_{\max}^\pm(t)\Phi^\pm(\zeta^\pm)$, where $\zeta^\pm = (s - s_r)\kappa_{\max}^\pm(t)$, s_r is the coordinate of the reconnecting point, and $\kappa_{\max}$ is the maximum value of curvature. The present calculations predict

$$\kappa_{\max}^\pm(t) \propto |t - t_r|^{-1/2}, \quad \frac{\kappa_{\max}^+(t)}{\kappa_{\max}^-(t)} = \left(\frac{A^+}{A^-}\right)^3. \tag{7}$$

Note that the $t^{-1/2}$ scaling could be directly inferred by dimensional analysis arguments but not the scaling of the dimensionless prefactors. Moreover, these self-similar functions $\Phi^\pm(\zeta^\pm)$ can be expressed in compact forms for small values of γ and $t - t_r$ as

$$\Phi^\pm(\zeta) = \frac{1}{\left\{1 + \left[\left(\frac{A^\mp}{A^\pm}\right)^2 + 1\right]\zeta^2\right\}^{3/2}} + O\left(\eta^\pm\gamma^2\frac{(t - t_r)}{\tau}\right), \tag{8}$$

with $\eta^\pm = (A^\mp/A^\pm)^2 - 1$. This function corresponds to a cusp in the vortex filament at $t = t_r$ and $s = s_r$. The dependence on the coefficient $(A^\mp/A^\pm)^2 + 1$ multiplying the self-similar variable $\zeta^\pm$ is unexpected and could not also be guessed by dimensional arguments. We also remark that the self-similarity is only exact when $\gamma = 0$ or $\eta^\pm = 0$.
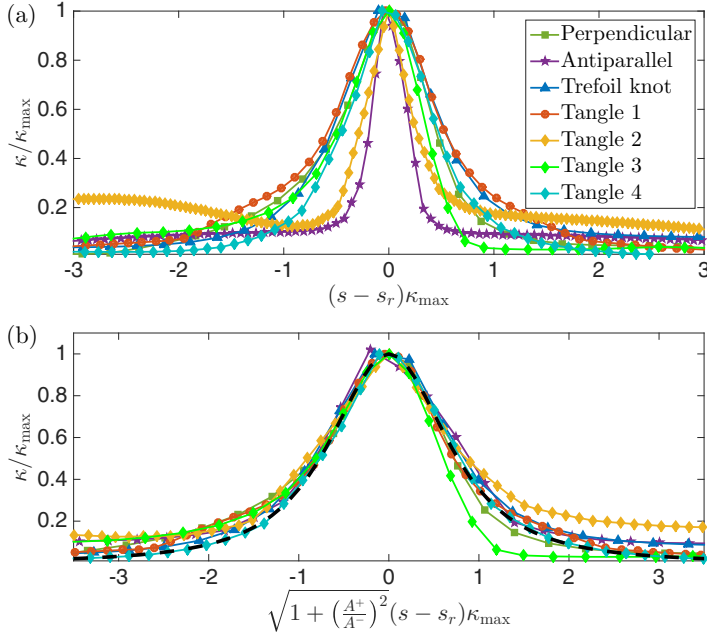
FIG. 4. (a) Curvature normalized by $\kappa_{\max}$ close to (just before) the reconnection time for all reconnection events explored as a function of $(s - s_r)\kappa_{\max}$. (b) Same data represented using the scaling suggested by the self-similar form (8). The black dashed line displays the theoretical prediction.

Finally, the torsion $\mathcal{T}^{\pm}(s,t)$ of the vortex line can also be computed within this approximation. When $\gamma \neq 0$ torsion is not identically null but it vanishes at s_r, thus confirming that reconnections occur locally on a plane. Also, it can be proved that it changes sign linearly at s_r with a slope that diverges as $\gamma|t - t_r|^{-1/2}$, creating shocklike structures. The slope ratio before and after the reconnection satisfies the relation $\frac{d\mathcal{T}^+}{ds}/\frac{d\mathcal{T}^-}{ds}|_{s=s_r} = A^+/A^-$.

We observe that in the context of Euler and Navier-Stokes flows, dynamical equations for torsion and curvature have been derived in Ref. [35]. These nonlinear equations do not allow for predicting the generation of curvature cusps and shocklike torsion structures. It would be interesting to investigate if the scaling laws reported above also remain valid in classical fluids and MHD flows.

V. NUMERICAL MEASUREMENTS OF THE CURVATURE AND TORSION

Motivated by the previous asymptotic results, we analyze the data coming from simulations. We start by looking at the curvature at a fixed time very close to the reconnection. In Fig. 4(a) the curvature just before t_r normalized using $\kappa_{\max}$ is shown for all configurations. We indeed observe the formation of a cusp at the reconnection point s_r in all cases. Note that, strictly speaking, no universal function of the curvature is observed. This is actually expected from the calculations of the curvature (8), which shows a dependence on the values A^+/A^- that differ from case to case. However, (8) suggests that if the variable $\sqrt{1 + (A^+/A^-)^2}(s - s_r)\kappa_{\max}$ is used instead, a universal form should be recovered. As shown in Fig. 4(b), the data indeed collapse into one universal function when using this new variable. The theoretical prediction (8) is also plotted with a dashed black line to appreciate the remarkable agreement.

We now study the temporal evolution of the curvature to determine if a self-similar evolution is observed. Figure 5(a) shows how the trefoil knot curvature curves, rescaled by their maximum values, almost perfectly collapse into a single plot, demonstrating the self-similar behavior for this
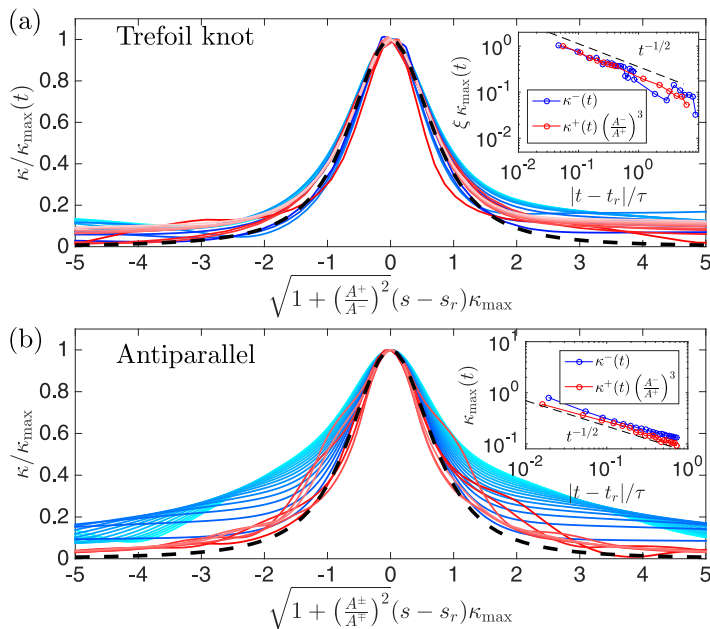
FIG. 5. (a) Self-similar evolution of the curvature close to the reconnection point for the trefoil vortex. Blue lines (from light to dark) correspond to times before reconnection and red lines (from dark to light) to times after reconnection. The inset displays the temporal evolution of the maximum value of the curvature on a log-log scale before and after, normalized as suggested in Eq. (7). (b) Same plot as in (a) but for the reconnection occurring in the antiparallel case. In both figures we consider times such that $|t - t_r| < 0.5\tau$ and the dashed line shows the $t^{-1/2}$ scaling. In both figures the black dashed line displays the theoretical prediction (8).

configuration. In the inset we plot the maximum value of the curvature as a function of time on a log-log scale. The predicted $t^{-1/2}$ scaling of (7) is clearly observed. In Fig. 5(b) we present the same analysis done for the antiparallel case where a clear breakdown of the self-similar behavior is observed. This can be explained by assuming a non-negligible value of γ, hence a strong torsion, that breaks the validity of the expansion done to obtain (8), only recovered when times are very close to t_r, as evident when comparing with the theoretical prediction displayed as a dashed black line. The temporal evolution of the maximum of curvature, shown in the inset of Fig. 4(b), still confirms the relations presented in Eq. (7), namely, the scaling $t^{-1/2}$ scaling normalized by the ratio of the prefactors is confirmed. Note that the agreement is very good given the large value $(A^+/A^-)^3 = 4.15^3$. For all other cases except tangle 2, self-similarity is observed (data not shown).

The breakdown of self-similarity is predicted by (8) when $A^+/A^- \neq 1$ and $\gamma \neq 0$. A nonzero value of γ is related, as we have seen, to torsion close to the reconnection point and a shocklike structure formation (see Appendix C). In Fig. 6(a) we show the temporal evolution of the torsion $\mathcal{T}$ for the antiparallel case. The shocklike structure formation, as well as the linear behavior close to the reconnection point, is clearly visible, thus explaining the breakdown of the self-similarity in Fig. 5(b). The inset shows that the temporal evolution of the slope of the torsion at s_r obeys the scaling $|t - t_r|^{-1/2}$ with the correct normalization A^+/A^- suggested by the analytical calculations. For completeness, in Fig. 6(b) we show the torsion normalized by the maximum value of the curvature for all the configurations close to the reconnection time. In all the other cases except for tangle 2, the slope of torsion is almost zero at the reconnection point. Remarkably, tangle 2 and antiparallel configurations correspond to the cases where vortices separate much faster than they approach [see Fig. 3(a)]. We remark finally that measuring quantities such as curvature and torsion is numerically very challenging as they involve high-order derivatives.
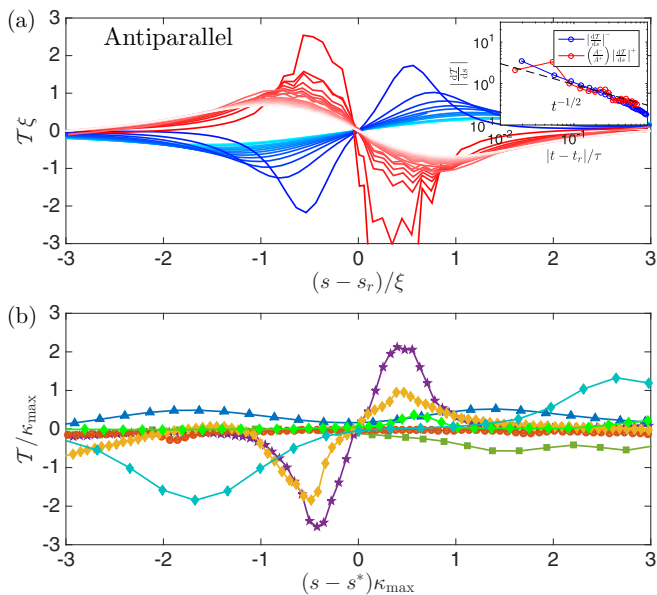
FIG. 6. (a) Temporal evolution of the torsion $\mathcal{T}$ as a function of the arc length in the antiparallel case. Blue lines (from light to dark) correspond to times before reconnection and red lines (from dark to light) to times after reconnection. The inset displays the temporal evolution of the slope of torsion computed at the reconnection point s_r on a log-log scale before and after, normalized as A^+/A^-. (b) Torsion $\mathcal{T}$ as a function of the arc length close to (just before) the reconnection for all configurations (same legend as in Fig. 4).

VI. DISCUSSION

The reconnection of quantized vortex filaments within the Gross-Pitaevskii model displays both universal and nonuniversal phenomena. We found that close to the reconnection the approach and separation rates follow the same scaling $\delta \sim (\Gamma t)^{1/2}$ and the vortex filaments always become locally antiparallel. Previous numerical studies reported scaling rates in the form of a power law with exponents depending on the configuration. By dimensional analysis, any scaling different from $\alpha = 1/2$ would introduce necessarily a new time or length scale to the problem that needs to be made explicit. The discrepancies in previous studies might be due to the fact that (i) the computational domain is not big enough, hence introducing a non-negligible system size length scale, (ii) the initial condition contains a considerable amount of sound waves such that the rms value of the compressible kinetic energy can be used to construct an extra time scale, or (iii) the observed scaling corresponds to dynamical regimes occurring much farther or later than the reconnection event and is thus driven by the specific vortex configuration and therefore is nonuniversal. In that spirit, reconnections within Navier-Stokes flows, a modified version of the model GP with nonlocal potential and/or high-order nonlinearities to better replicate superfluid liquid helium, or coupled GP equations modeling multicomponent or spinorial BECs could indeed lead to different scalings.

Our findings demonstrate that the prefactors $A^{\pm}$ are not universal in the GP method. However, once measured case by case, their ratio determines many properties of the reconnection dynamics. Note that the easiest way to determine this ratio is to look at the medium- to large-scale reconnection angle ϕ between the hyperbola asymptotes, which should be an accessible quantity in superfluid experiments [11,13,36]. Let us also remark that the $t^{1/2}$ scaling we observed extends beyond the distance ξ. This suggests that the linear approximation might be used as a matching theory in order to relate measurements done well before and far from the reconnection events. Bose-Einstein

condensate experimentalists are able today to study vortex dynamics and reconnections [13,36]. Our predictions should directly apply to those systems.

Finally, let us underline that understanding the dynamics of the reconnection events is crucial to provide a full comprehension of the dissipative processes occurring in superfluids in the low-temperature limit. It is largely believed that Kelvin waves play a fundamental role carrying the energy to the smallest scales where it finally gets dissipated by sound radiation. The cusps arising in the vortex filaments due to reconnection events are responsible for a rapid and efficient excitation of Kelvin waves at all scales. Here we provided an analytical formula for the dynamical formation of the cusps and we aim to use this result in further theoretical studies to estimate the rate of radiation during reconnection. Also, we have shown that non-negligible torsion of the reconnecting filaments implies the breakdown of self-similarity, resulting in the formation of shocklike structures of the torsion. This phenomenon seems to be linked to the large difference observed in the $A^{\pm}$ prefactors, hence to extreme events where vortices separate much faster than they approach, and to the irreversibility of the reconnection events. We do not have yet a theoretical understanding of this fact and more data would be desirable to perform a detailed statistical analysis.

ACKNOWLEDGMENTS

APPENDIX A: THE GROSS-PITAEVSKII EQUATION

In the limit of very low temperature a weakly interacting Bose gas can be described using a mean field approximation in terms of a complex order parameter (or condensate wave function) ψ. Such a system is governed by a dispersive nonlinear wave equation called the Gross-Pitaevskii equation

$$i\hbar \frac{\partial \psi}{\partial t} = -\frac{\hbar^2}{2m}\nabla^2\psi + g|\psi|^2\psi - \mu\psi, \tag{A1}$$

where m is the mass of the bosons and $g = 4\pi a\hbar^2/m$, with a the boson s-wave scattering length. The chemical μ can in principle be absorbed by a global phase shift. Although formally derived for BECs, the GP model qualitatively reproduces many aspects of superfluid liquid helium too. It can be used to model classical vortex dynamics in situations where a large-scale separation between the vortex core and the size of such a vortex is present.

The GP equation possesses a Hamiltonian structure and conserves the total number of particles

$$N = \int |\psi|^2 d^3\mathbf{x}, \tag{A2}$$

the total energy

$$H = \int \left(\frac{\hbar^2}{2m}|\nabla\psi|^2 + \frac{g}{2}|\psi|^4\right)d^3\mathbf{x}, \tag{A3}$$

and the total momentum

$$\mathbf{P} = \frac{\hbar}{2i}\int [\psi^*\nabla\psi - \psi\nabla\psi^*]d^3\mathbf{x}. \tag{A4}$$

The speed of sound for such a model is given by $c = \sqrt{g\rho_0}/m$. This value can be derived by linearizing (A1) about a constant value $\psi = \sqrt{\rho_0/m} = \sqrt{\mu/g}$. It is also possible to identify a characteristic length $\xi = \hbar/\sqrt{2\rho_0 g}$, called healing length, representing the scale where the linear contribution in Eq. (A1) equals the nonlinear one. Dispersive effects will then take place for length scales smaller than ξ. Equation (A1) can be rewritten in term of the two physical quantities c and ξ as

$$i\frac{\partial \psi}{\partial t} = \frac{c}{\sqrt{2}\xi}\left(-\xi^2 \nabla^2 \psi - \psi + \frac{m}{\rho_0}|\psi|^2 \psi\right). \tag{A5}$$

By using the Madelung transformation

$$\psi(\mathbf{x},t) = \sqrt{\frac{\rho(\mathbf{x},t)}{m}}e^{i[\varphi(\mathbf{x},t)/\sqrt{2}c\xi]}, \tag{A6}$$

it possible to relate the order parameter ψ to a compressible, irrotational, and barotropic superfluid having density $\rho(\mathbf{x},t)$ and velocity $\mathbf{v} = \nabla\varphi$. Indeed, plugging the transformation (A6) into (2), we directly obtain

$$\frac{\partial \rho}{\partial t} + \nabla \cdot (\rho\mathbf{v}) = 0, \tag{A7}$$

$$\frac{\partial \phi}{\partial t} + \frac{1}{2}\mathbf{v}^2 = c^2\frac{\rho_0 - \rho}{\rho_0} + c^2\xi^2\frac{\nabla^2\sqrt{\rho}}{\sqrt{\rho}}. \tag{A8}$$

Equations (A7) and (A8) are the continuity equation and the Bernoulli equation, respectively, except for the last term in Eq. (A8), which is called quantum pressure and has no analog in classical fluid mechanics.

Although the velocity field defined by the Madelung transformation (A6) is potential, solutions with nonzero circulation can exist in the form of topological defects of the order parameter ψ. For such vortex solutions the vorticity is supported on the curves (nodal lines) where the density field vanishes and the phase is not defined. In order to ensure that the order parameter stays single valued, the circulation around such nodal lines must be constant and equal to a multiple of the Onsager-Feynman quantum of circulation $\Gamma = h/m = 2\sqrt{2}\pi c\xi$. For this reason, nodal lines of the order parameter are called quantum (or quantized) vortices. The region around the topological defect where the density drops to zero is called the vortex core and its size is of the order of the healing length ξ. The hydrodynamical interpretation of superfluids is thus the one of a compressible (dispersive) flow where vorticity is a distribution (a superposition of Dirac δ's) supported on the vortex filament.

We would like to remark that often quantum vortices are misleadingly referred to as the singularities of the system, as the velocity field diverges as $1/r$, where r is the distance to the filament. This divergence is just a consequence of the change of coordinates given by the Madelung transformation. At the vortex position, the order parameter solution of the GP equation is a smooth field. We can thus precisely track vortices finding the zeros of ψ as described in Appendix B.

APPENDIX B: VORTEX TRACKING ALGORITHM

We have recently developed a robust and accurate algorithm to track vortex lines of the order parameter ψ in arbitrary geometries. The details of the algorithm and accuracy of the method can be found in Ref. [29]. We recall here the basic ideas. A quantized vortex line in three dimensions corresponds to a nodal line defined by

$$\text{Re}[\psi(x,y,z)] = \text{Im}[\psi(x,y,z)] = 0. \tag{B1}$$

The algorithm is based on a Newton-Raphson method to find zeros of ψ and on the knowledge of the *pseudovorticity* field $\mathbf{W} = \nabla \text{Re}[\psi] \times \nabla \text{Im}[\psi]$, always tangent to the filaments, to follow vortex lines [18]. Starting from a point $\mathbf{x}_0$ where the density $|\psi|^2$ is below a given small threshold (therefore
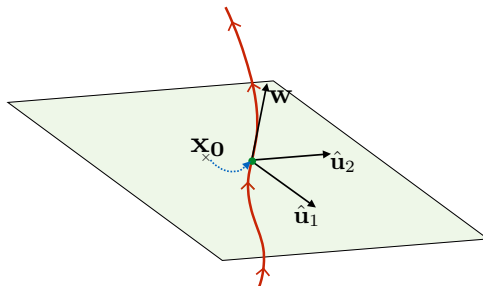
FIG. 7. Sketch of the plane on which the Newton-Raphson method is implemented.

very close to a vortex), we define the orthogonal plane to the vortex line using $\mathbf{W}(\mathbf{x}_0)$. The plane is then spanned by the two directors $\hat{\mathbf{u}}_1$ and $\hat{\mathbf{u}}_2$, as illustrated in Fig. 7. A better approximation for the vortex position $\mathbf{x}_v$ on the plane is then given by $\mathbf{x}_1 = \mathbf{x}_0 + \delta\mathbf{x}$. Here the increment $\delta\mathbf{x}$ is obtained using the Newton-Raphson formula (the linear approximation)

$$0 = \psi(\mathbf{x}_0 + \delta\mathbf{x}) \approx \psi(\mathbf{x}_0) + J(\mathbf{x}_0)\delta\mathbf{x}, \tag{B2}$$

where $J(\mathbf{x}_0)$ is the Jacobian matrix expressed as

$$J = \begin{pmatrix} \nabla\,\mathrm{Re}[\psi]\cdot\hat{\mathbf{u}}_1 & \nabla\,\mathrm{Re}[\psi]\cdot\hat{\mathbf{u}}_2 \\ \nabla\,\mathrm{Im}[\psi]\cdot\hat{\mathbf{u}}_1 & \nabla\,\mathrm{Im}[\psi]\cdot\hat{\mathbf{u}}_2 \end{pmatrix}. \tag{B3}$$

The increment can be therefore calculated using $\delta\mathbf{x} = -J^{-1}(\mathbf{x}_0)\cdot\{\mathrm{Re}[\psi(\mathbf{x}_0)],\mathrm{Im}[\psi(\mathbf{x}_0)]\}^T$. Sufficiently close to the line, the Jacobian matrix is always a nonsingular 2×2 matrix, so its inverse can be computed. We underline that the method requires the evaluation of the Jacobian (B3) at intermesh points. Making use of the spectral representation of ψ, we can precisely compute those values using Fourier transforms. This process can be iterated until the exact location $\mathbf{x}_v$ is determined upon a selected convergence precision.

To track the following vortex point of the same line we use as a next initial guess $\mathbf{x}_0 = \mathbf{x}_v + \zeta\mathbf{W}$, which is obtained evolving along $\mathbf{W}$ by a small step ζ. The process is reiterated until the entire line is tracked and closed and then repeated with another line until the whole computation domain has been fully explored.

APPENDIX C: DETAILED CALCULATIONS OF THE LINEAR APPROXIMATION

An analytical study of a reconnection event in the GP model was provided by Nazarenko and West [15], where it is shown that two vortices are antiparallel during a reconnection and their distance scales as $\delta(t) \sim t^{1/2}$. In the same spirit as [15], we assume that inside the vortex core the nonlinear term of the GP equation can be neglected and so a reconnection event should be governed by the (linear) Schrödinger equation. For the sake of simplicity, in dimensionless units this equations reads

$$i\partial_t\psi + \tfrac{1}{2}\nabla^2\psi = 0. \tag{C1}$$

Note that we absorbed the parameters c and ξ in Eq. (2) by a suitable time and space rescaling. We remark that in Ref. [15] reconnections are studied just on a plane, whereas here we consider vortex filaments with nonzero torsion. At the reconnection time t_r we use as the initial condition the ansatz

$$\psi_r(x,y,z) = z + \frac{\gamma}{a}(x^2 + y^2) + i(az + \beta x^2 - y^2). \tag{C2}$$

Looking for $\psi_r = 0$, one can recover the vortex profile, given by the curves

$$\mathbf{R}(s) = \left(s, \pm s\sqrt{\frac{\beta - \gamma}{\gamma + 1}}, -s^2\frac{\gamma(\beta + 1)}{a(\gamma + 1)}\right), \tag{C3}$$
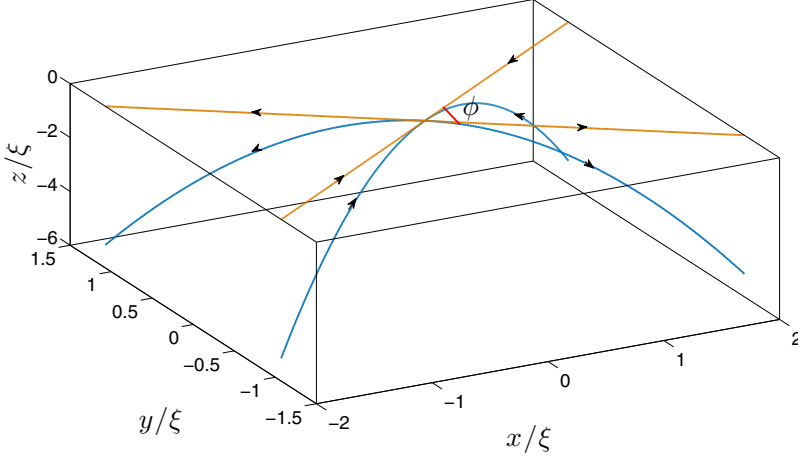
FIG. 8. Plot of the initial condition using $\gamma = 0.01$, $\beta = 1/2$, and $a = 1$. The vortex filaments are shown in blue while their projection on the x-y is shown in orange. The arrows identify the circulation around each vortex.

where s is the parametrization of the curve. We note that (C3) requires that

$$\frac{\beta - \gamma}{\gamma + 1} > 0. \tag{C4}$$

In Fig. 8 we plot the vortex filaments $\mathbf{R}(s)$ (blue lines) for our initial condition.

The vortices projected on the x-y planes form two hyperbola (orange lines) crossing at the reconnection point. We note that the values β and γ fix the angle

$$\phi = 2 \tan^{-1}\left(\sqrt{\frac{1 + \gamma}{\beta - \gamma}}\right) \tag{C5}$$

between the two hyperbola. The arrows identify the circulation around each vortex.

The formal solution of Eq. (C1) is given by

$$\psi(t) = e^{i[(t - t_r)\nabla^2/2]}\psi_r, \tag{C6}$$

where t_r is the time when the reconnection occurs. The choice of a second-order polynomial for ψ_r allows us to find the exact solution of (C1):

$$\psi(t) = z + \frac{\gamma}{a}(x^2 + y^2) - 2t(\beta - 1) + i\left(az + \beta x^2 - y^2 + 4(t - t_r)\frac{\gamma}{a}\right). \tag{C7}$$

Assuming $a > 0$ and $\gamma < \beta < \frac{a^2 - 2\gamma}{a^2}$, the vortex lines before the reconnection ($t < t_r$) are given by

$$\mathbf{R}_{1,2}^-(s,t) = \left(s, \pm\sqrt{\frac{(t_r - t)(a^2(1 - \beta) - 2\gamma) + as^2(\beta - \gamma)}{a(\gamma + 1)}}, \right.$$
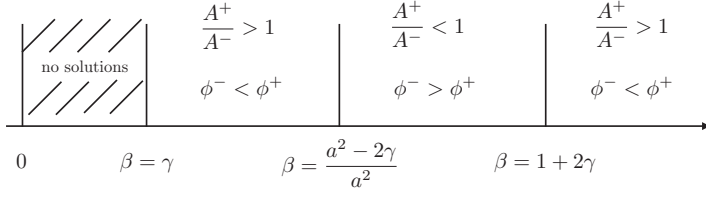$$\left. \frac{(t - t_r)(a^2(\beta - 1) - 2\gamma^2) - a\gamma(\beta + 1)s^2}{(\gamma + 1)a^2}\right), \tag{C8}$$

FIG. 9. Dependence of the ratio $\frac{A^+}{A^-}$ and the angles ϕ^- and ϕ^+ on different values of β.

while after the reconnection $(t > t_r)$

$$\mathbf{R}^+_{1,2}(s,t) = \left(\pm \sqrt{\frac{(t - t_r)(a^2(1 - \beta) - 2\gamma) + as^2(1 + \gamma)}{a(\beta - \gamma)}}, s, \right.$$
$$\left. \frac{(t - t_r)(a^2(\beta - 1) + 2\gamma^2) - a\gamma(\beta + 1)s^2}{(\beta - \gamma)a^2} \right). \tag{C9}$$

From the above curves we observe that the two vortices approach along the y direction and separate along the x direction. It follows that

$$\delta^\pm(t) = |\mathbf{R}^\pm_1(0,t) - \mathbf{R}^\pm_2(0,t)| = \sqrt{2\pi} A^\pm |t - t_r|^{1/2}, \tag{C10}$$

where the ratio of prefactors satisfies

$$\frac{A^+}{A^-} = \sqrt{\frac{1 + \gamma}{\beta - \gamma}} > 1. \tag{C11}$$

From Eq. (C5) we can see how the quantity $\frac{A^+}{A^-}$ is related to the angle ϕ. Calling ϕ^- the angle of the approaching vortices and ϕ^+ the angle of the separating vortices, we can conclude that for $\beta < \frac{a^2 - 2\gamma}{a^2}$, $\phi^- > \phi^+$. On the other hand, when $\beta > \frac{a^2 - 2\gamma}{a^2}$ the two vortices approach along the x direction and separate along the y direction with $\frac{A^+}{A^-} = \sqrt{\frac{\beta - \gamma}{1 + \gamma}}$. For the sake of completeness, in Fig. 9 we show the values of the ratio $\frac{A^+}{A^-}$ and the angles ϕ^- and ϕ^+ for different values of β. We note that $\frac{A^+}{A^-} < 1$ for $\frac{a^2 - 2\gamma}{a^2} < \beta < 1 + 2\gamma$, while $\frac{A^+}{A^-} > 1$ for $\beta > 1 + 2\gamma$.

As a final remark, we note that changing the sign of a corresponds to looking at the reconnection back in time, hence each value of $\frac{A^+}{A^-}$ in Fig. 9 will then be reversed. The linear approximation also allows for computing the curvature

$$\kappa(s,t) = \frac{|\mathbf{R}'(s,t) \times \mathbf{R}''(s,t)|}{|\mathbf{R}'(s,t)|^3} \tag{C12}$$

and torsion

$$\mathcal{T}(s,t) = \frac{[\mathbf{R}'(s,t) \times \mathbf{R}''(s,t)] \cdot \mathbf{R}'''(s,t)}{|\mathbf{R}'(s,t) \times \mathbf{R}''(s,t)|^2} \tag{C13}$$

of the vortex lines.

The curvature can be directly evaluated. Its maxima as a function of time before and after reconnection are given by

$$\kappa^-_{\max}(t) \sqrt{\frac{4\gamma^2(1 + \beta)^2[a^2(\beta - 1) + 2\gamma](t - t_r) + a^3(\beta - \gamma)^2(1 + \gamma)}{a^2(1 + \gamma)^2[a^2(\beta - 1) + 2\gamma](t - t_r)}} \tag{C14}$$
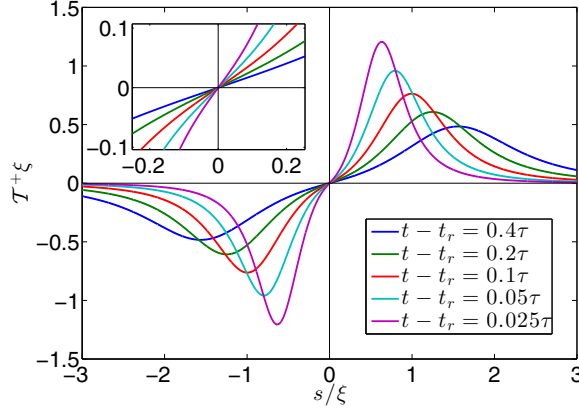
FIG. 10. Plot of the torsion versus the y coordinate, for different time steps using $\gamma = 0.01$, $\beta = 1/2$, and $a = 1$.

and

$$\kappa_{max}^+(t) = \sqrt{\frac{4\gamma^2(1+\beta)^2[a^2(\beta-1)+2\gamma](t-t_r) - a^3(\beta-\gamma)^2(1+\gamma)^2}{a^2(\beta-\gamma)[a^2(\beta-1)+2\gamma](t-t_r)}}, \qquad \text{(C15)}$$

respectively. The present calculation predicts $\kappa_{max}^\pm(t) \propto |t - t_r|^{-1/2}$, which also corresponds to a dimensional analysis prediction. In addition, the linear approximation predicts that $\kappa_{max}^+/\kappa_{max}^- = (A^+/A^-)^3$ in the limit of $t \to t_r$. This nontrivial result cannot be found by dimensional arguments. Moreover, one can show that $\kappa^\pm$ presents a self-similar behavior close to the reconnection point of the form $\kappa^\pm(s,t) = \kappa_{max}^\pm(t)\Phi^\pm(\zeta_\pm)$, where $\zeta^\pm = (s - s_r)\kappa_{max}^\pm(t)$ and s_r is the coordinate of the reconnecting point. For small values of γ, these self-similar functions can be found to be

$$\Phi^\pm(\zeta) = \frac{1 \pm \frac{3}{2}\frac{(\beta^{\pm 1}+1)\zeta^2}{1+(\beta^{\pm 1}+1)\zeta^2}\gamma}{[1+(\beta^{\pm 1}+1)\zeta^2]^{3/2}} + O(\gamma^2) = \frac{1}{\left\{1 + \left[\left(\frac{A^\mp}{A^\pm}\right)^2 + 1\right]\xi^2\right\}^{3/2}} + O\left(\eta^\pm \gamma^2 \frac{(t-t_r)}{\tau}\right),$$

$$\text{(C16)}$$

where $\eta^\pm = (A^\mp/A^\pm)^2 - 1$. Remarkably, once the ratio A^+/A^- is reintroduced, γ only appears as a quadratic correction to the self-similar form. Note that within this approximation, self-similarity is destroyed when $\eta^\pm \gamma^2 (t-t_r)/\tau$ is of order 1.

We note that if one chooses $\beta > \frac{a^2-2\gamma}{a^2}$, then $\frac{A^+}{A^-} = \sqrt{\frac{\beta-\gamma}{1+\gamma}}$ and

$$[\Phi^\pm(\zeta)]_{\beta>(a^2-2\gamma)/a^2} = [\Phi^\mp(\zeta)]_{\beta<(a^2-2\gamma)/a^2}. \qquad \text{(C17)}$$

The former calculations were evaluated using symbolic computation software.

Finally, the torsion $\mathcal{T}^\pm(s,t)$ of the vortex line can be also computed within this approximation. It vanishes at s_r (suggesting a locally planar reconnection); however, it changes sign linearly at this point. Its slope is given by

$$\frac{d\mathcal{T}^+}{ds} = -\gamma \frac{3\sqrt{2}(1+\beta)}{\sqrt{a(\beta-\gamma)}\sqrt{(t-t_r)[a^2(1-\beta)-2\gamma]}} \qquad \text{(C18)}$$

and it diverges as $\gamma|t - t_r|^{-1/2}$. The torsion thus develops shocklike structures as displayed in Fig. 10.

The inset in Fig. 10 shows the linear behavior close to the reconnection point. It is possible to prove analytically that the ratio of the slopes is given by $\frac{d\mathcal{T}^+}{ds}/\frac{d\mathcal{T}^-}{ds}|_{s=s_r} = A^+/A^-$. The full formulas for the torsion are too long to be presented here.

[1] E. R. Priest, in *Proceedings of the VIIth International Conference on Plasma Astrophysics and Space Physics, Lindau, 1998*, edited by J. Büchner, I. Axford, E. Marsch, and V. Vasyliūnas (Springer Netherlands, Dordrecht, 1999), pp. 77–100.

[2] S. Kida and M. Takaoka, Vortex reconnection, Annu. Rev. Fluid Mech. **26**, 169 (1994).

[3] J. Koplik and H. Levine, Vortex Reconnection in Superfluid Helium, Phys. Rev. Lett. **71**, 1375 (1993).

[4] X. Zhike, Y. Xiaoli, C. Xin, Y. Liheng, S. Yingna, K. Bernhard, Z. Jun, L. Zhong, B. Yi, X. Yongyuan, Y. Kai, and Z. Li, Observing the release of twist by magnetic reconnection in a solar filament eruption, Nat. Commun. **7**, 11837 (2016).

[5] F. Hussain and K. Duraisamy, Mechanics of viscous vortex reconnection, Phys. Fluids **23**, 021701 (2011).

[6] E. Fonda, D. P. Meichle, N. T. Ouellette, S. Hormoz, and D. P. Lathrop, Direct observation of Kelvin waves excited by quantized vortex reconnection, Proc. Natl. Acad. Sci. USA **111**, 4707 (2014).

[7] P. Constantin, C. Fefferman, and A. J. Majda, Geometric constraints on potentially singular solutions for the 3-D Euler equations, Commun. Part. Diff. Eq. **21**, 559 (1996).

[8] H. K. Moffatt, The interaction of skewed vortex pairs: A model for blow-up of the Navier-Stokes equations, J. Fluid Mech. **409**, 51 (2000).

[9] R. P. Feynman, in *Progress in Low Temperature Physics*, edited by C. J. Gorter (Elsevier, Amsterdam, 1955), Chap. 2, pp. 17–53.

[10] K. W. Schwarz, Three-dimensional vortex dynamics in superfluid ^{4}He: Homogeneous superfluid turbulence, Phys. Rev. B **38**, 2398 (1988).

[11] G. P. Bewley, M. S. Paoletti, K. R. Sreenivasan, and D. P. Lathrop, Characterization of reconnecting vortices in superfluid helium, Proc. Natl. Acad. Sci. USA **105**, 13707 (2008).

[12] B. P. Anderson, P. C. Haljan, C. A. Regal, D. L. Feder, L. A. Collins, C. W. Clark, and E. A. Cornell, Watching Dark Solitons Decay into Vortex Rings in a Bose-Einstein Condensate, Phys. Rev. Lett. **86**, 2926 (2001).

[13] S. Serafini, M. Barbiero, M. Debortoli, S. Donadello, F. Larcher, F. Dalfovo, G. Lamporesi, and G. Ferrari, Dynamics and Interaction of Vortex Lines in an Elongated Bose-Einstein Condensate, Phys. Rev. Lett. **115**, 170402 (2015).

[14] A. W. Baggaley, L. K. Sherwin, C. F. Barenghi, and Y. A. Sergeev, Thermally and mechanically driven quantum turbulence in helium II, Phys. Rev. B **86**, 104501 (2012).

[15] S. Nazarenko and R. West, Analytical solution for nonlinear Schrödinger vortex reconnection, J. Low Temp. Phys. **132**, 1 (2003).

[16] S. Zuccher, M. Caliari, A. W. Baggaley, and C. F. Barenghi, Quantum vortex reconnections, Phys. Fluids **24**, 125108 (2012).

[17] A. J. Allen, S. Zuccher, M. Caliari, N. P. Proukakis, N. G. Parker, and C. F. Barenghi, Vortex reconnections in atomic condensates at finite temperature, Phys. Rev. A **90**, 013601 (2014).

[18] C. Rorai, J. Skipper, R. M. Kerr, and K. R. Sreenivasan, Approach and separation of quantised vortices with balanced cores, J. Fluid Mech. **808**, 641 (2016).

[19] A. T. A. M. de Waele and R. G. K. M. Aarts, Route to Vortex Reconnection, Phys. Rev. Lett. **72**, 482 (1994).

[20] R. Tebbs, A. J. Youd, and C. F. Barenghi, The approach to vortex reconnection, J. Low Temp. Phys. **162**, 314 (2011).

[21] D. Kivotides, J. C. Vassilicos, D. C. Samuels, and C. F. Barenghi, Kelvin Waves Cascade in Superfluid Turbulence, Phys. Rev. Lett. **86**, 3080 (2001).

[22] S. Nazarenko, Kelvin wave turbulence generated by vortex reconnections, JETP Lett. **84**, 585 (2007).

[23] R. Hänninen, Kelvin waves from vortex reconnection in superfluid helium at low temperatures, Phys. Rev. B **92**, 184508 (2015).

[24] M. W. Scheeler, D. Kleckner, D. Proment, G. L. Kindlmann, and W. T. M. Irvine, Helicity conservation by flow across scales in reconnecting vortex links and knots, Proc. Natl. Acad. Sci. USA **111**, 15350 (2014).

[25] Y. Kimura and H. K. Moffatt, Reconnection of skewed vortices, J. Fluid Mech. **751**, 329 (2014).

[26] C. E. Laing, R. L. Ricca, and L. S. De Witt, Conservation of writhe helicity under anti-parallel reconnection, Sci. Rep. **5**, 9224 (2015).

[27] S. Zuccher and R. L. Ricca, Helicity conservation under quantum reconnection of vortex rings, Phys. Rev. E **92**, 061001 (2015).

[28] P. Clark di Leoni, P. D. Mininni, and M. E. Brachet, Helicity, topology, and Kelvin waves in reconnecting quantum knots, Phys. Rev. A **94**, 043605 (2016).

[29] A. Villois, G. Krstulovic, D. Proment, and H. Salman, A vortex filament tracking method for the Gross-Pitaevskii model of a superfluid, J. Phys. A: Math. Theor. **49**, 415502 (2016).

[30] N. G. Berloff and P. H. Roberts, Motion in a Bose condensate: IX. Crow instability of antiparallel vortex pairs, J. Phys. A: Math. Gen. **34**, 10057 (2001).

[31] D. Proment, M. Onorato, and C. F. Barenghi, Vortex knots in a Bose-Einstein condensate, Phys. Rev. E **85**, 036306 (2012).

[32] C. Nore, M. Abid, and M. E. Brachet, Decaying Kolmogorov turbulence in a model of superflow, Phys. Fluids **9**, 2644 (1997).

[33] A. Villois, D. Proment, and G. Krstulovic, Evolution of a superfluid vortex filament tangle driven by the Gross-Pitaevskii equation, Phys. Rev. E **93**, 061103 (2016).

[34] See Supplemental Material at http://link.aps.org/supplemental/10.1103/PhysRevFluids.2.044701 for an explanatory movie of the knot reconnection.

[35] P. Constantin, I. Procaccia, and D. Segel, Creation and dynamics of vortex tubes in three-dimensional turbulence, Phys. Rev. E **51**, 3207 (1995).

[36] S. Serafini, L. Galantucci, E. Iseni, T. Bienaimé, R. N. Bisset, C. F. Barenghi, F. Dalfovo, G. Lamporesi, and G. Ferrari, Vortex reconnections and rebounds in trapped atomic Bose-Einstein condensates, arXiv:1611.01691.